

Dynamical Evolution of Rotating Stellar Systems: III. The Effect of Mass Spectrum

Eunhyeuk Kim^{1,2*}, Hyung Mok Lee^{1†}, and Rainer Spurzem^{3‡}

¹*Astronomy Program, SEES, Seoul National University, Seoul 151-742, Korea*

²*Harvard-Smithsonian Center for Astrophysics, 60 Garden Street, Cambridge, MA 02138, USA*

³*Astronomisches Rechen-Institut, Mönchhof-Strasse 12-14, 69120 Heidelberg, Germany*

30 October 2018

ABSTRACT

We have studied the dynamical evolution of rotating star clusters with mass spectrum using a Fokker-Planck code. As a simplest multi-mass model, we first investigated the two-component clusters. Rotation is found to accelerate the dynamical evolution through the transfer of angular momentum outward, as well as from the high masses to the low masses. However, the degree of acceleration depends sensitively on the assumed initial mass function since dynamical friction, which generates mass segregation, also tends to accelerate the evolution, and the combined effect of both is not linear or multiplicative. As long as dynamical friction dominates in the competition with angular momentum exchange the heavy masses lose random energy and angular momentum, sink towards the centre, but their remaining angular momentum is sufficient to speed them up rotationally. This is gravo-gyro instability. As a consequence, we find that the high mass stars in the central parts rotate faster than low mass stars. This leads to the suppression of mass segregation compared to the non-rotating clusters. From the study of multi-component models, we observe similar trends to the two-component models in almost all aspects. The mass function changes less drastically for clusters with rotation. Unlike non-rotating clusters, the mass function depends on R and z . Our models are the only ones that can predict mass function and other quantities to be compared with new observations.

Key words: celestial mechanics, stellar dynamics – globular clusters: general

1 INTRODUCTION

Since the pioneering studies of Lupton & Gunn (1987) and its subsequent applications to fit actual globular cluster observations it is evident that galactic globular clusters exhibit some degree of rotation, and that there is also a consistent amount of observed flattening of their shapes (White & Shawl 1987). More recently, van Leeuwen et al. (2000) and Anderson & King (2003) measure globular cluster rotation in proper motion, in order to derive the true direction of its rotational axis. Though not dominant the amount of rotational energy could also not be neglected on the other hand side, as was seen by the models of Einsel & Spurzem, which showed that even a moderate fraction of rotational energy in a cluster leads to significantly faster core evolution.

This is the third in a series of studies on the dynamical

evolution of rotating stellar system by using orbit-averaged 2D Fokker-Planck (FP) models that include the effects of initial rotation. In the previous two papers, pre-collapse evolution (Einsel & Spurzem 1999, Paper I) and the evolution after core-collapse (Kim et al. 2002, Paper II) of rotating clusters composed of equal mass stars were studied. In the present study we explore the dynamical evolution of the rotating stellar systems with mass spectrum as a natural extension to the previous works. We expect that the exchange of angular momentum between different mass species would significantly affect the course of dynamical evolution, as the energy exchange is known to play important role in the evolution of multi-mass clusters.

Direct integration of the Fokker-Planck equation is used as a statistical method. Comparisons between results obtained with FP method and results from N -body simulation show that the approximations and assumptions which were used in FP models are reasonable, but need to be checked carefully by comparison of different methods. The simplest implementation of an FP model is a one-dimensional (1D) FP model where the distribution function f is assumed to

* e-mail: ekim@cfa.harvard.edu

† e-mail: hmlee@astro.snu.ac.kr

‡ e-mail: spurzem@ari.uni-heidelberg.de

depend only on the energy E of stars. All physical properties depend on the distance from the cluster center only (Cohn 1980; Lee, Fahlman & Richer 1991). The use of 1D models is inspired by the fact that the shape of globular clusters is approximately spherical, but it ignores the anisotropy of the velocity dispersion. Observations of globular clusters and theoretical models suggested that there exists a difference in the velocity dispersion between radial and tangential direction, especially for stars in the outer regions of the clusters (Takahashi 1995, 1996, 1997). The two-dimensional FP model where distribution function depends on energy and angular momentum with spherical geometry has been pioneered by Cohn (1979) but studied extensively only recently because of difficulties in numerical integration of the equations (Takahashi, Lee & Inagaki 1997, Takahashi & Lee 2001). In our case, modelling axisymmetric systems with only two integrals requires a careful check in particular. Any third integral is neglected here completely, which means that the diffusion properties of orbits in the axisymmetric potential are treated as a function of two integrals only.

Although there are successes in previous FP models to explain the dynamical evolution of star clusters, only few of them considered the natural and important physical property of the existence of an initial angular momentum in the star cluster. Kim et al. (2002) have reviewed briefly the previous studies where the initial rotation is considered. They presented the first post-core collapse studies on the evolution of rotating stellar systems and found that the global shape of the rotational structure of the globular cluster changes little, though the strength of the rotation (measured using the magnitude of the rotational velocity or the z -component of the angular momentum) decreases continuously with time due to the outward transfer of the angular momentum. An incorporation of mass loss and enhanced two-body relaxation processes accelerated the evolution of the star cluster not only in core-collapse time, but also the dissolution time of the cluster. They found an approach to self-similar evolution in late core-collapse.

The previous studies where the initial rotation is considered, assumed a star cluster with equal mass stars. Inclusion of the initial mass spectrum known to change the evolution of star clusters significantly, shortening of core-collapse times for example (Lee, Fahlman & Richer 1991). We also expect that there may be important physical processes between different mass species concerning the exchanges of the angular momentum. Until now, no study has been done on rotating star clusters with mass spectrum except for one preliminary work by Spurzem & Einsel (1998). In this paper, thus we present the study of dynamical evolution of the rotating star cluster with the initial mass function (IMF hereafter). We first investigate the evolution of two-component models as a simplest extension of the single mass models. Then we extend our study to the multi-mass models represented by ten different mass species. The difference of our models as compared to the preliminary work by Spurzem & Einsel (1998) is that first our improved code includes more accurate numerical integration and discretisation procedures as described in Paper II, and here we do an extensive parameter study, which did not exist before.

The outline of the present paper is as follows; In section 2, the FP equations for the multi-mass system and the initial models are presented. We concentrate on the evolution up

to the core collapse of two component models in section 3 and multi-mass models in section 4. We further discuss the evolution beyond the core collapse for both two-component and multi-component models section 5. We summarize our main results in section 6.

2 THE MODELS

2.1 Fokker-Planck Equations

We have constructed a computational scheme to study the dynamical evolution of rotating stellar systems with mass spectrums in detail with higher accuracy both for pre- and post-collapse. The framework of the method is essentially an extension of the method used in Paper II. The multi-mass FP equation under a fixed potential can be written in a flux-conserving form as follows:

$$P(E, J_z) \frac{\partial f_i}{\partial t} = -\frac{\partial F_{E_i}}{\partial E} - \frac{\partial F_{J_z, i}}{\partial J_z} \quad (1)$$

where $P(E, J_z)$ is the phase space volume accessible for stars with E and J_z , and f_i , F_{E_i} and $F_{J_z, i}$ are the distribution function and the particle flux in energy (E) and z -component of angular momentum (J_z) of the i -th component, respectively. The expression for phase space volume is given in Paper I. The particle fluxes F_{E_i} and $F_{J_z, i}$ can be expressed as follows:

$$\begin{aligned} -F_{E_i} &= D_{EE, i} \frac{\partial f_i}{\partial E} + D_{EJ_z, i} \frac{\partial f_i}{\partial J_z} + D_{E, i} f_i, \\ -F_{J_z, i} &= D_{J_z J_z, i} \frac{\partial f_i}{\partial J_z} + D_{J_z E, i} \frac{\partial f_i}{\partial E} + D_{J_z, i} f_i. \end{aligned} \quad (2)$$

where $D_{EE, i}$, $D_{EJ_z, i}$, etc are the diffusion coefficients and are given in the Appendix of Paper I for single component models. The extension to the multi-mass models can be simply done by applying the distribution function of the i -th component in the expression of these coefficients.

It is necessary to add energy source to explore the evolution after core-collapse. Primordial binaries and massive stars are important energy sources, since they can delay significantly the core-collapse time and change the early evolution of stellar systems (Gao et al. 1991, Giersz & Spurzem 2000). However, the specification of primordial binaries could introduce many more model parameters. The treatment of such binaries in FP code is not so trivial either. Since we are mainly concerned with the general effects of rotation on the dynamical evolution of star clusters, we limit ourselves to simplest cases. As a way to follow the dynamical evolution beyond the core collapse, we have only considered the heating effect of binaries formed by three-body processes. Heating formula for three-body binaries of Lee, Fahlman & Richer (1991) is used in our models (see also Takahashi 1997 for the discussion of this formula). In their formulation, the total heating rate per unit volume is given by

$$\dot{E}_{tot} = C_i G^5 \left(\sum_i \frac{n_i m_i^2}{\sigma_i^3} \right)^3 \sigma_0^2 \quad (3)$$

where n_i , m_i , and σ_i are the number density, stellar mass, and one-dimensional velocity dispersion, respectively, of the i -th component, and σ_0 is the mass density-weighted central one-dimensional velocity dispersion. The standard value of $C_b = 90$ is used for present study. Heating rate for each mass component is obtained by distributing the total heating rate such that

$$\dot{E}_{tot,i} = \frac{\rho_i}{\rho_{tot}} \dot{E}_{tot} \quad (4)$$

where ρ_i and ρ_{tot} represent mass density of each component and total density. Giersz & Spurzem (1997) have demonstrated that such a simple approximations work very well for modelling the post-collapse evolution of globular clusters.

2.2 Multi-Mass Initial Models

We employ the rotating King models as initial models following Lupton & Gunn (1987). We assume that there is no initial mass segregation among different mass species. Our present initial models are, therefore simple extension of the initial models used in Papers I and II. These models are characterized by two parameters: dimensionless central potential W_0 and rotational parameter ω_0 . We have studied the evolution of clusters with $W_0 = 6$ and $W_0 = 3$, respectively. Model clusters are assumed to rotate in circular orbits around mother galaxy, so that the mean density within the tidal radius (r_t) remains a constant throughout the evolution. We examined the evolution of clusters with various amount of the initial rotations (see Tables 1 and 2 for the list of the initial models of two component, and multi-component, respectively).

First, we considered the models with two-component mass species. Two-component models are expected to provide us with understanding the essential features of the evolution of the multi-component clusters (for example, the transfer of angular momentum between two mass components). We have examined the wide range of individual stellar mass ratio $\mu := m_2/m_1$ and total mass ratio $M_1/M_2 = (1 - q)/q$, where $q := M_2/(M_1 + M_2)$. The quantities μ and q can be compared with the work of Khalisi (2002) and Fregeau et al. (2002).

Next, we considered clusters which have continuous mass spectra. We choose simple power-law mass function for convenience. The number of stars in a mass interval ($m, m + dm$) is given by

$$dN(m) = Cm^\alpha dm, \quad m_{\min} \leq m \leq m_{\max} \quad (5)$$

where m_{\min} and m_{\max} denote the minimum and the maximum masses, respectively. The dynamic range of mass spectrum, expressed as m_{\max}/m_{\min} is 10 for present study.

We have studied the evolution of clusters with three different shapes of mass function: $\alpha = -1.20, -2.35$ and -3.50 , where $\alpha = -2.35$ represents Salpeter-type mass function. We list the parameters of the models with continuous mass spectrum in Tables 1 and 2. For models of post core-collapse, we consider only a model with a mass function with $\alpha = -2.35$.

The number of mass groups used in present study is ten. The mass of each group is assigned such that

Table 1. Initial Models of clusters with $W_0 = 6$.

Model	m_2/m_1	M_1/M_2	α_0	ω_0	$T_r/T_k(0)$ [%]	Phase
M2A	2	5	-	0.0	0.00	Pre
				0.2	3.40	Pre
				0.3	7.06	Pre
				0.4	11.35	Pre
				0.6	20.17	Pre
				0.8	27.96	Pre
				1.0	34.23	Pre
M2B	2	10	-	0.0	0.00	Pre
				0.3	7.06	Pre
				0.6	20.17	Pre
				0.0	0.00	Post
				0.3	7.06	Post
M2C	5	10	-	0.6	20.17	Post
				0.0	0.00	Pre
				0.3	7.06	Pre
M2D	5	100	-	0.6	20.17	Pre
				0.0	0.00	Pre
				0.3	7.06	Pre
M2E	10	10	-	0.6	20.17	Pre
				0.0	0.00	Pre
				0.3	7.06	Pre
M2F	10	100	-	0.6	20.17	Pre
				0.0	0.00	Pre
				0.3	7.06	Pre
MCA	-	-	-1.20	0.6	20.17	Pre
				0.3	7.06	Pre
				0.0	0.00	Pre
MCB	-	-	-2.35	0.6	20.17	Post
				0.3	7.06	Post
				0.0	0.00	Post
MCC	-	-	-3.50	0.6	20.17	Pre
				0.3	7.06	Pre
				0.0	0.00	Pre

T_r : total rotational energy

T_k : total kinetic energy

$$m_i = m_{\min} \left(\frac{m_{\max}}{m_{\min}} \right)^{(i-\frac{1}{2})/10}, \quad (i = 1, 2, \dots, 10). \quad (6)$$

The total mass of i th mass group is

$$M_i = \int_{m_{i-\frac{1}{2}}}^{m_{i+\frac{1}{2}}} N(m) m dm. \quad (7)$$

If the initial density distribution and the initial mass function including m_{\min} and m_{\max} are fixed, the only free parameter for the model is the number of stars (or total mass if the masses of stars are given in physical units). The general behavior of the core collapse does not depend on the number of stars. However, the core stops to collapse and begins to expand when the central density exceeds a certain value which depends on the total number of stars in

Table 2. Initial Models of clusters with $W_0 = 3$.

Model	m_2/m_1	M_1/M_2	α_0	ω_0	$T_r/T_k(0)$ [%]	Phase
M2A	2	5	–	0.0	0.00	Pre
				0.4	1.89	Pre
				0.8	6.96	Pre
				1.2	13.84	Pre
				1.5	19.37	Pre
1.6	21.20	Pre				
M2B	2	10	–	0.0	0.00	Pre
				0.8	6.96	Pre
				1.5	19.37	Pre
M2C	5	10	–	0.0	0.00	Post
				0.8	6.96	Post
				1.5	19.37	Post
M2D	5	100	–	0.0	0.00	Pre
				0.8	6.96	Pre
				1.5	18.37	Pre
M2E	10	10	–	0.0	0.00	Pre
				0.8	6.96	Pre
				1.5	19.37	Pre
M2F	10	100	–	0.0	0.00	Pre
				0.8	6.96	Pre
				1.5	19.37	Pre
MCA	–	–	–1.20	0.0	0.00	Pre
				0.8	6.96	Pre
				1.5	19.37	Pre
MCB	–	–	–2.35	0.0	0.00	Post
				0.8	6.96	Post
				1.5	19.37	Post
MCC	–	–	–3.50	0.0	0.00	Pre
				0.8	6.96	Pre
				1.5	19.37	Pre

the cluster. If N is too small, we cannot apply the Fokker-Planck method to follow the evolution of the star cluster. The development of gravothermal oscillation occurs for N much larger than 10,000 because the post-collapse cluster becomes gravothermally unstable (Goodman 1987). The use of larger N also takes more computational time because the post-collapse expansion begins at much higher central density. As a compromise, we have used $N = 10,000$ for models in the present study.

The number of stars used here is quite small compared to that of globular clusters. According to the recent comparisons between direct N -body models and the Fokker-Planck models (Takahashi & Portegies Zwart 1998, Portegies Zwart & Takahashi 1999) the evolution of the total mass until total dissolution depends on the particle number since the mass loss process involves the crossing time rather than the relaxation time. Nevertheless we restrict ourselves here to post-collapse models using relatively small N , because this speeds up the computational time, and we are mainly interested in the interplay between rotation, relaxation and tidal mass loss. $N = 10,000$ is large enough to study the effect of the

core bounce due to the formation of binaries. Aside from the actual values of the central density, the general behavior of the post-collapse evolution does not sensitively depend on initial N . Note that there will be rapid core oscillation, which is beyond the scope of the present study, if we use realistic particle numbers.

2.3 Tidal Boundary

All models studied in the present work are tidally limited. Realistic treatment of tidal field is possible only for direct N -body calculations. The simplest assumption for the tidal boundary is to assume a spherical shape whose radius is determined by the requirement of constant mean density within this radius. The actual shape is not exactly spherical and the tidal field varies with time as the cluster moves along non-circular orbit in non-spherical Galactic potential. Nevertheless, we assumed a constant mean density within the tidal radius for simplicity.

We have applied the “energy condition” for the removal of stars (see Takahashi, Lee & Inagaki 1997 for details of tidal conditions). Takahashi & Portegies Zwart (1998) found that the “apocenter condition” reproduces the result of the N -body simulation better for small N models, but the difference between different conditions diminishes as N becomes larger. Since our distribution functions do not depend on total angular momentum, we could not apply the apocenter condition. However, we emphasize that our choice of $N = 10,000$ is simply to reduce the computational time. Although the parameters for the central parts (central density, core radius and central velocity dispersion) are sensitive to the N , the global evolution (such as $M(t)$, $r_h(t)$) do not depend on N as long as we use large N approximation for the tidal conditions. We could consider our results to be appropriate for systems with very large N , except for the core properties.

3 PRE-COLLAPSE EVOLUTION OF TWO-COMPONENT MODELS

Under the context of our models of two-body relaxation, rotation, and binary heating the clusters always go through the core-collapse and begins the post-collapse expansion. Some aspects of the evolution differ between pre- and post-collapse phases. Thus we first discuss the pre-collapse evolution of two-component models first. In the study of the pre-collapse phase only, we have ignored the heating by binaries.

For clusters with multiple mass, the energy exchange between different mass species causes mass segregation which takes place in a time scale shorter than the single-mass core-collapse. Once the core is dominated by the massive component whose velocity dispersion is lower than average, the core collapse proceeds more rapidly than the single component clusters. The rotation is also known to accelerate the core-collapse process since it provides additional mechanism of driving the catastrophic collapse. In two-component clusters, these two processes compete with each other. We now investigate how the rotation affects the course of core-collapse of two-component models.

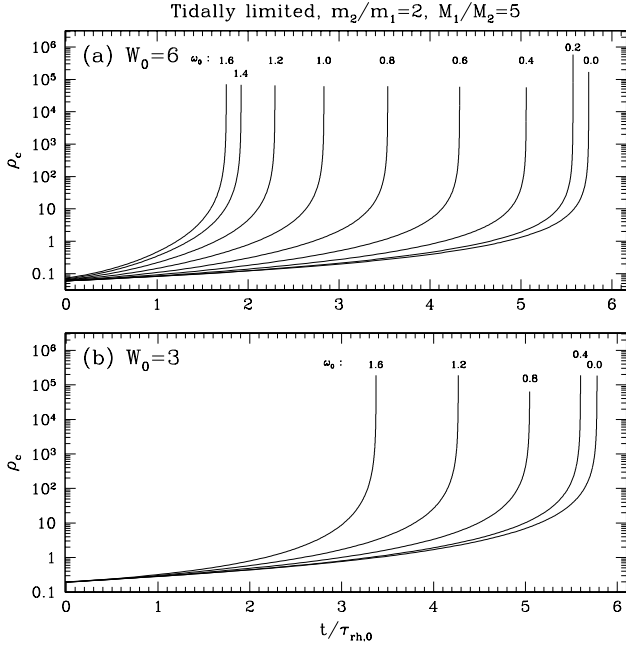


Figure 1. Time evolution of the central density for the cluster model with mass function M2A

3.1 Central density and core-collapse time

We have shown the evolution of central density for the model M2A with different initial central potential, $W_0 = 3$ and 6 in Fig. 1. The time is expressed in units of the initial half-mass relaxation time ($\tau_{rh,0}$), and the central density in units of $M_0/r_{c,0}^3$, where M_0 and $r_{c,0}$ are the initial mass of the cluster and the initial King’s core radius, respectively. An expression for the initial half-mass relaxation time is taken from Spitzer & Hart (1971),

$$\tau_{rh,0} = \frac{0.138 N_0^{1/2} r_{h,0}^{1/2}}{G^{1/2} \bar{m}^{1/2} \ln \Lambda} \quad (8)$$

where N_0 , $r_{h,0}$, G , \bar{m} and $\ln \Lambda$ denote the initial total number of stars the initial half-mass radius, gravitational constant, the mean mass of the particles and the Coulomb logarithm, respectively. Since the rotating clusters are not spherically symmetric, some cautions should be taken in defining the half-mass radius. It is defined as the effective radius of concentric spheroid within which the enclosed mass becomes half of the total mass (see eq. [22] of Einsel & Spurzem 1999).

It is shown clearly that the clusters with higher initial rotation reach core-collapse earlier than the cluster without initial rotation. In order to quantify the amount of acceleration of the evolution, we define the “degree of acceleration” as follows:

$$d_{acc} \equiv \frac{t_{cc}(\omega = 0) - t_{cc}(\omega)}{t_{cc}(\omega)}, \quad (9)$$

where t_{cc} is the time to reach the core-collapse. Obviously, d_{acc} depends on ω for a given W_0 and a mass function. We have listed d_{acc} in the last column of Tables 3 and 4, and have shown them in Fig. 2(b).

Fig. 2(a) shows the run of the core-collapse times as a function of the initial rotation (solid line) and the ratio

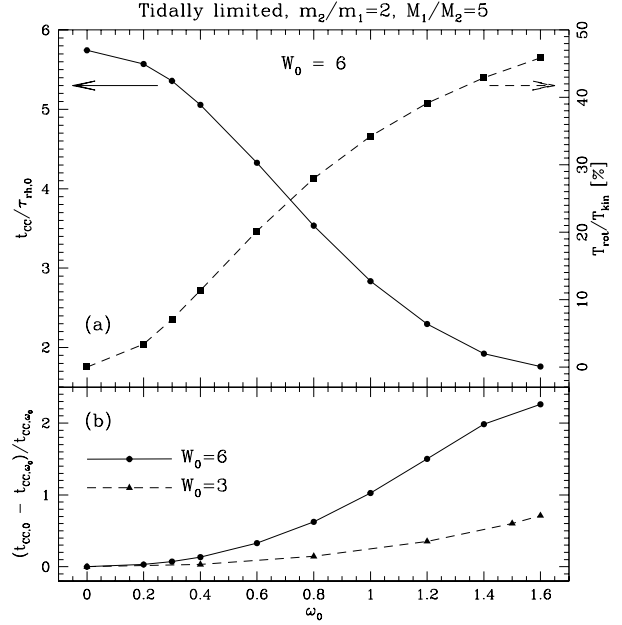


Figure 2. (a) Run of core collapse time measured in initial half mass relaxation time as a function of the initial rotation parameter (ω_0) for a series of models with a mass function M2A and $W_0 = 6$ (solid line). A ratio between the initial rotational energy and the total kinetic energy for the same models (dashed line). (b) The degree of the acceleration of core-collapse defined by eq. 9 for model with the central potential $W_0 = 6$ (solid line) and 3 (dashed line), respectively.

between initial total rotational energy due to the rotation and initial total kinetic energy (dashed line) for model with mass function of M2A and the initial central potential $W_0 = 6$. The ratio between rotational energy and kinetic energy of the model with initial rotation $\omega_0 = 1.6$ is $\sim 46\%$, just below the dynamically unstable criterion of $T_r/T_k = 0.5$, where T_r and T_k denote the total rotational energy and total kinetic energy. The core-collapse times, which are measured in units of the initial half-mass relaxation time decrease as the initial degree of rotation increases. The cluster with the initial rotation $\omega_0 = 0.6$ reaches the core collapse faster by a factor of ~ 1.3 than the cluster without the initial rotation. The cluster with the initial rotation $\omega_0 = 1.6$, a model with the largest initial degree of rotation among current models, has a core-collapse time of just $\sim 1/3$ of that of the model without the initial rotation.

We have shown the time evolution of central density for models with different mass function except for mass function of M2A in Fig. 3. Solid lines represent the models without initial rotation. Dotted lines and dashed lines represent the models with the initial degree of rotation $\omega_0 = 0.3$ and 0.6 , respectively. We have chosen the values for the initial degree of rotation as the same values used in Paper II. The mass ratios between high and low mass components (m_2/m_1) and the ratios of total masses of these components (M_1/M_2) are written to distinguish the different mass functions.

In general the core collapse occurs earlier for more rapidly rotating models. The degrees of acceleration also depends sensitively on the assumed mass function. For ex-

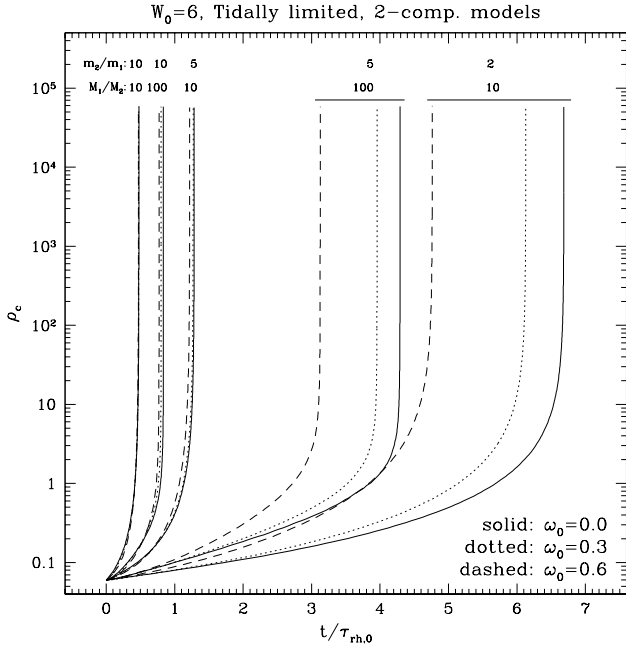


Figure 3. Time evolution of the central density for the cluster model with two-component mass functions and $W_0 = 6$ except for a mass function of M2A.

ample, d_{acc} of the model with the initial rotation $\omega_0 = 0.6$ and mass function of M2B is much larger than that of the model with mass function M2E, which has the same initial degree of rotation. The main difference between these two models is the ratio of the individual mass: $m_2/m_1 = 2$ for M2B and 10 for M2E. The larger difference in individual mass means larger amount of energy exchange and thus the significant amount of acceleration of core collapse due to this effect alone. There appears not enough room for the acceleration due to the initial rotation for such cases. For a given m_2/m_1 , the degree of acceleration also depends on M_1/M_2 . If the total mass in high mass component is relatively large (i.e., smaller values for M_1/M_2), the acceleration due to rotation is small. Such trend can be seen from the comparison between M2C and M2D or M2E and M2F. For models with relatively small M_1/M_2 , the acceleration due to mass segregation is already significant and the role of rotation is relatively less important.

Time evolution of total mass of the clusters with mass function M2A is displayed in Fig. 4. The total mass of each mass component is normalized by their initial total mass $M_{i,0}$. The dashed lines represent the total mass of lighter component and the solid lines for massive component, respectively. The total mass of lighter component decreases more rapidly than the that of massive stars, irrespective of the initial degree of rotations. The cluster with a initially higher rotation loses mass more efficiently than the clusters with lower initial rotation. The higher mass-loss rate of cluster with the higher initial rotation was known in previous works for single mass models (Papers I and II). The ratio of total masses at a time of core-collapse between two mass components varies with different initial degree of rotations. For the model with initial rotation of $\omega_0 = 1.6$, the total mass of the low mass component at the time of core-collapse

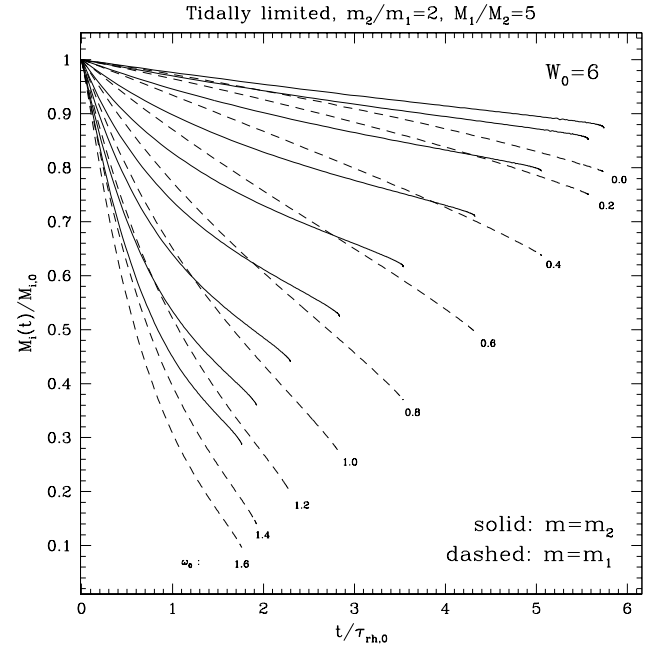


Figure 4. Evolution the total masses retained in a cluster for model with $W_0 = 6$ and mass function M2A. The total mass of the individual component is normalized by its initial total mass $M_{i,0}$. Solid lines represent the evolution for the massive stars and dashed lines for the less massive stars, respectively.

is $\sim 10\%$ of its initial value. On the other hand, $\sim 30\%$ of the initial mass still remains for massive component. The ratio of total mass at a time of core-collapse between the high and low mass components for model without the initial rotation is ~ 1.1 , which is much lower than the value obtained for cluster model with the initial rotation $\omega_0 = 1.6$. It implies that the mass function of rotating cluster which has the same initial mass function will follow different evolution according to their initial rotation. The evolution of mass function, especially the power law index α , for models with initially power-law mass function is explained in detail in Sect. 5.4.

3.2 Central velocity dispersion and central angular speed

Einsel & Spurzem (1999) argued in their single mass model that the acceleration of core-collapse time for models with the initial rotation compared to the model without the initial rotation is accompanied by a rapid increase of the central velocity dispersion in rotating models. We have checked if this is also true for two component models. Fig. 5 shows the evolution of mass density weighted central one-dimensional velocity dispersion (σ_c) for models with the central potential $W_0 = 6$ and mass function model of M2A. The initial rotational parameters (ω_0) are written in front of the starting points of evolution.

The evolution of σ_c measured in the total central density (ρ_c) shows a rather complex behavior. For models with large initial rotation, σ_c increases in the very early phase of evolution and then decrease until it reaches broad minimum.

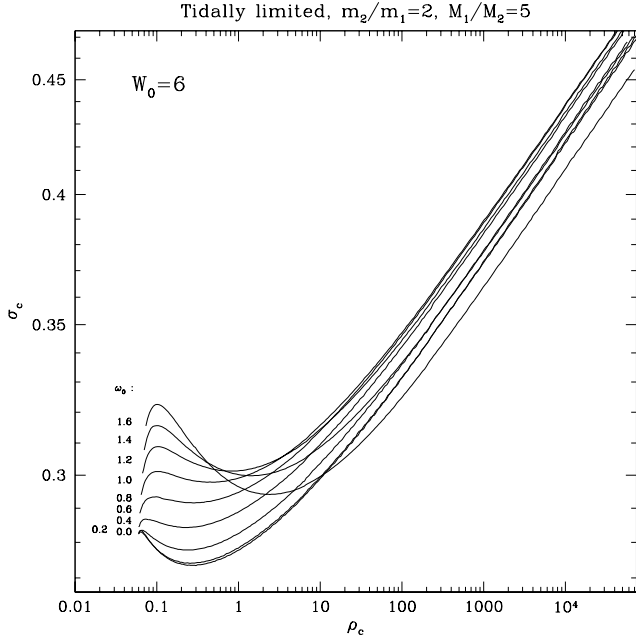


Figure 5. Evolution of the mass-weighted central 1D velocity dispersion with respect to the central density for cluster models with $W_0 = 6$ and M2A for a mass function. The values of initial rotational parameter (ω_0) are written ahead of the starting points of the evolution.

Eventually, σ_c increases with ρ_c monotonically toward the core collapse.

The initial rise of σ_c is caused by the initial collapse and subsequent heating by contraction. The decrease of σ_c after the local maximum is due to the loss of energy of high mass stars to low mass stars. Since there are more low mass stars in the early phase in the central parts, the mass-weighted velocity dispersion decreases. The subsequent increase of σ_c after the broad minimum occurs when the central part is dominated by high mass stars. The stars in the central parts lose energy to stars in the outer parts and the velocity dispersion increases because of the negative specific heat.

The evolutionary path reaches self-similar collapse phase when the central density increases by 2 \sim 3 orders of magnitude. The evolution of self-similar collapse can be characterized by a parameter given by

$$\gamma = \frac{d \ln \sigma_c^2}{d \ln \rho_c}. \quad (10)$$

For single mass system, Einsel & Spurzem (1999) obtained an average value of $\gamma = 0.109$, independent of the initial degree of rotation. It is expected that γ for present two component models is very similar to that of the single component system, since the central part of cluster is dominated by high mass stars. We derive an average value of $\gamma = 0.105$, which is very similar to what was obtained for single mass model.

Another feature of Fig. 5 is the initial evolution of σ_c depends on the amount of initial rotation. The minima occur at higher central density for models with larger initial rotation. The enhanced two-body relaxation process due to rotation will eventually cause more rapid increase the central

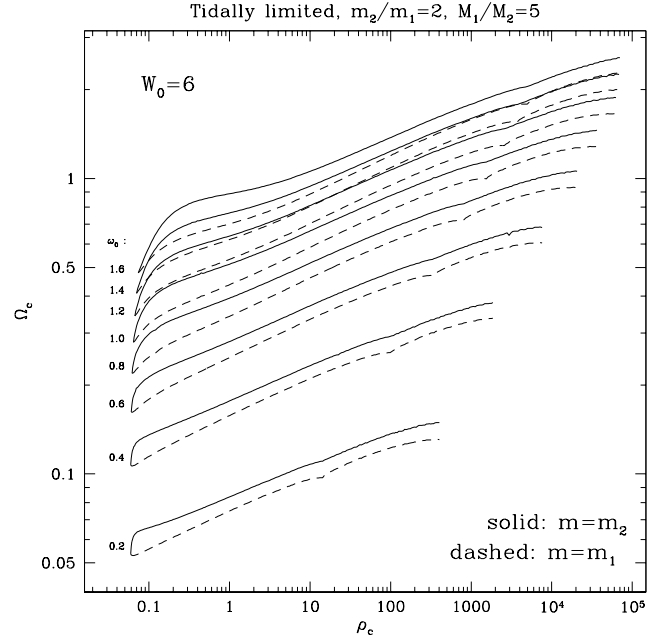


Figure 6. Evolution of the central angular speed of the individual mass species with respect to the total central density for cluster models with $W_0 = 6$ and M2A for a mass function. The central rotational speed of the massive stars (solid lines) increases very fast during the early evolutionary stage, while that of the lighter stars (dashed lines) shows an moderate increase.

density. This results in the acceleration of the core-collapse for rapidly rotating systems.

Fig. 6 displays the run of central angular speed (Ω_c) as a function of the total central density for the model with the mass function of M2A. The solid lines and the dashed lines represent Ω_c of high mass and low mass components, respectively. It is shown clearly that Ω_c of the higher mass component increases very quickly only during early phase of evolution. For the models rotating slowly ($\omega_0 = 0.2$ and 0.4) Ω_c of lower mass component decreases by a small amount. For rapidly rotating clusters, however, Ω_c increases with increase of central density. The rapid increase of Ω_c of high mass component in the early phase is a caused by rapid collapse of the high mass stars: as they lose energy, they rotate faster.

The mass weighted angular speeds in the core as a function of ρ_c for the models in Fig. 6 are shown in Fig. 7. During early evolution, Ω_c increases rapidly for models with large rotation, then it grows slowly with increase of central density, reaching self-similar phase in evolutionary path. Einsel & Spurzem (1999) introduced the parameter δ which characterizes the self-similar evolution of central angular speed as follows,

$$\delta = \frac{d \ln \Omega_c}{d \ln \rho_c}. \quad (11)$$

The calculated values of δ for the present two-component models are listed in Table 3. On average, $\delta \approx 0.110$ with weak dependence on the initial rotation for model

Table 3. Physical properties of cluster models with $W_0 = 6$.

Model	ω_0	$t_{CC}/\tau_{rh,0}$	M_{CC}/M_0	$t_{dis}/\tau_{rh,0}$	d_{acc}	γ	δ
M2A	0.0	5.74	0.81	–	0.00	0.108	–
	0.2	5.57	0.78	–	0.03	0.114	0.112
	0.3	5.36	0.72	–	0.07	0.106	0.114
	0.4	5.06	0.66	–	0.14	0.106	0.113
	0.6	4.33	0.53	–	0.33	0.105	0.111
	0.8	3.54	0.41	–	0.62	0.105	0.108
	1.0	2.83	0.31	–	1.03	0.105	0.108
	1.2	2.30	0.24	–	1.50	0.105	0.111
	1.4	1.92	0.18	–	1.99	0.105	0.109
1.6	1.76	0.13	–	2.26	0.106	0.107	
M2B	0.0	6.69	0.78	–	0.00	0.106	–
	0.3	6.13	0.70	–	0.09	0.105	0.108
	0.6	4.76	0.52	–	0.40	0.104	0.111
M2C	0.0	1.28	0.96	10.68	0.00	0.106	–
	0.3	1.27	0.93	7.74	0.01	0.105	0.090
	0.6	1.22	0.82	4.36	0.05	0.104	0.092
M2D	0.0	4.29	0.88	–	0.00	0.101	–
	0.3	3.96	0.82	–	0.08	0.099	0.092
	0.6	3.13	0.67	–	0.37	0.102	0.094
M2E	0.0	0.48	0.98	–	0.00	0.106	–
	0.3	0.47	0.97	–	<0.01	0.105	0.090
	0.6	0.47	0.90	–	0.01	0.104	0.084
M2F	0.0	0.84	0.98	–	0.00	0.099	–
	0.3	0.80	0.96	–	0.05	0.099	0.099
	0.6	0.77	0.90	–	0.08	0.101	0.100
MCA	0.0	3.49	0.83	–	0.00	0.106	–
	0.3	3.39	0.74	–	0.03	0.104	0.095
	0.6	2.83	0.54	–	0.23	0.103	0.099
MCB	0.0	1.98	0.92	9.60	0.00	0.104	–
	0.3	1.92	0.86	7.11	0.03	0.103	0.105
	0.6	1.72	0.70	4.16	0.15	0.103	0.113
MCC	0.0	1.73	0.94	–	0.00	0.098	–
	0.3	1.68	0.90	–	0.03	0.096	0.105
	0.6	1.55	0.77	–	0.12	0.096	0.103

$t_{CC}/\tau_{rh,0}$: core collapse time measured in the initial half-mass relaxation time
 M_{CC}/M_0 : mass of the cluster in unit of the initial total mass (M_0) at $t = t_{CC}$
 $t_{dis}/\tau_{rh,0}$: time in unit of $\tau_{rh,0}$ when the cluster dissolved completely
 γ, δ : see the text for the definitions.

M2A. This value of δ is about twice of those of single mass models. Einsel & Spurzem (1999) obtained $\delta = 0.06 \sim 0.08$ depending on the initial rotation for their model cluster with central potential $W_0 = 6$.

The relationship between the central density, σ_c , and Ω_c for models with mass function M2E ($m_2/m_1 = 10, M_1/M_2 = 10$) are shown in Fig. 8. For σ_c versus ρ_c , we have plotted the velocity dispersion of individual mass component for model without initial rotation and models with $\omega_0 = 0.3$ and 0.6 , while only the rotating models are shown for Ω_c versus ρ_c plot. The starry mark in Fig. 8(a) represents the starting point of evolution for both mass components. The central velocity dispersion of high mass component decreases dramatically, while that of low mass component increases slightly at early evolutionary stage due to the energy

equipartition between two mass components. The decrease of the central velocity dispersion for model with higher initial rotation is larger than that of the lower initial rotation. Inspection of Fig. 8(a) reveals that the slope in log-log plot for massive component becomes $\gamma \approx 0.105$ regardless of degree of rotation.

3.3 Rotational Velocity and Angular Momentum

Two-body relaxation causes the outward transfer of the angular momentum and escape of stars at the outer parts, leading to the decrease of rotational energy. Kim et al (2002) showed that the maximum value of rotational velocity ($V_{rot,max}$) in equator decreases monotonically for their single mass models. In Fig. 9, we displayed the evolution of

Table 4. Initial Models of clusters with $W_0 = 3$.

Model	ω_0	$t_{CC}/\tau_{rh,0}$	M_{CC}/M_0	$t_{dis}/\tau_{rh,0}$	d_{acc}	γ	δ
M2A	0.0	5.78	0.42	–	0.00	0.107	–
	0.4	5.60	0.39	–	0.03	0.106	0.110
	0.8	5.05	0.33	–	0.15	0.106	0.112
	1.2	4.27	0.25	–	0.35	0.106	0.113
	1.5	3.61	0.18	–	0.60	0.106	0.109
	1.6	3.37	0.15	–	0.71	0.106	0.111
M2B	0.0	6.21	0.41	–	0.00	0.105	–
	0.8	5.37	0.33	–	0.16	0.104	0.107
	1.5	3.79	0.19	–	0.64	0.104	0.113
M2C	0.0	1.98	0.76	4.17	0.00	0.105	–
	0.8	1.88	0.66	3.43	0.05	0.104	0.094
	1.5	1.59	0.39	2.01	0.25	0.105	0.090
M2D	0.0	4.82	0.57	–	0.00	0.104	–
	0.8	4.82	0.49	–	0.18	0.103	0.095
	1.5	2.80	0.34	–	0.72	0.104	0.099
M2E	0.0	0.86	0.87	–	0.00	0.105	–
	0.8	0.84	0.80	–	0.02	0.104	0.084
	1.5	0.76	0.56	–	0.13	0.104	0.085
M2F	0.0	1.54	0.86	–	0.00	0.102	–
	0.8	1.49	0.79	–	0.03	0.101	0.087
	1.5	1.37	0.60	–	0.13	0.101	0.093
MCA	0.0	4.01	0.38	–	0.00	0.104	–
	0.8	3.51	0.30	–	0.14	0.105	0.106
	1.5	2.51	0.15	–	0.60	0.105	0.103
MCB	0.0	2.65	0.56	4.18	0.00	0.102	–
	0.8	2.42	0.45	3.48	0.09	0.101	0.142
	1.5	1.83	0.23	2.31	0.45	0.103	0.139
MCC	0.0	2.48	0.70	–	0.00	0.096	–
	0.8	2.29	0.58	–	0.08	0.096	0.118
	1.5	1.82	0.34	–	0.36	0.096	0.135

maximum rotational speed at equator, where the effect of the rotation is largest, for model with the central potential $W_0 = 6$ and mass function M2A. Only four different models for initial degree of rotation is plotted to avoid complexity. Different line styles represent the different initial rotations. The thick lines represent the run of maximum rotational velocity at equator for the high mass component, and the thin lines for low mass component. The maximum rotational speed of low mass component decreases with the central density. The central density increases with time monotonically for core-collapse models as shown in Sect. 3.1. The rotational speed for the high mass component, especially for model with the initial degree of rotation $\omega_0 = 0.3$ increases during early evolutionary stage, and it remains around 0.2 afterward. However, the maximum rotational speed for rapidly rotating model (i.e., $\omega_0 = 1.6$) decreases with central density monotonically for both components. We have shown the run of the maximum rotational speed at equator for models with the central potential $W_0 = 6$ and $\omega_0 = 0.6$ in Fig. 10. To investigate the difference in rate of angular momentum transfer between two mass components, we include 6 different mass function models. The individual mass

ratio (m_2/m_1) and the total mass ratio (M_1/M_2) of initial model are marked in the figure. While the maximum rotation speeds of the high mass component increases slightly for model with lowest individual mass ratio ($m_2/m_1 = 2$), it increase more steeply for other models. The maximum rotational velocity of high mass component for models with $m_2/m_1 = 5$ and 10 remains a nearly constant afterward.

Kim et al. (2002) found that the specific angular momentum ($J_{z,\max}$) decreases with time for models with central King's potential $W_0 = 6$. Fig. 11 shows the evolution of maximum specific angular momentum with the increase of central density for the same models to those of Fig. 10. The line style and the thickness of each line represent the same mass function model shown in Fig. 10. The maximum angular momentum decreases monotonically irrespective of the mass function and the mass component, although the rate of decrease depends on the individual mass ratio and the mass components.

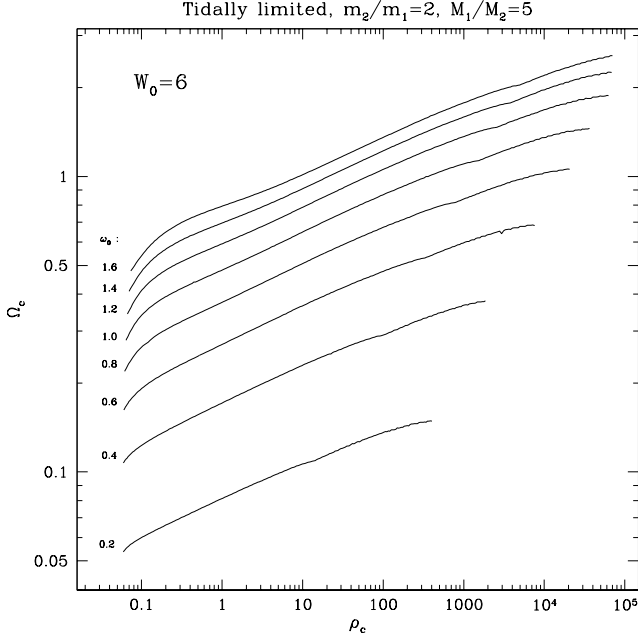


Figure 7. Evolution of the mass-weighted central angular speed with respect to the central density for cluster models with $W_0 = 6$ and M2A for a mass function.

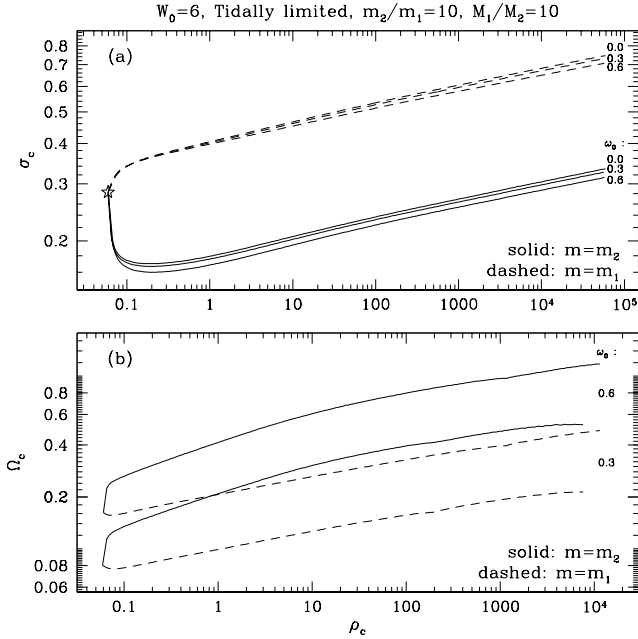


Figure 8. Evolution of the central velocity dispersion (a) and the central angular speed (b) for the models with $W_0 = 6$ and a mass function M2E ($m_2/m_1 = 10, M_1/M_2 = 10$), respectively. The start of the evolution is marked with starry mark in figure (a). We have included models with the initial rotation of $\omega_0 = 0.0, 0.3$ and 0.6 . However, only the rotating models are considered in Ω_c versus ρ_c plot. The steep decreasing of the central velocity dispersion and the steep rising for central angular speed of the massive component are shown clearly. The loss of central velocity dispersion is compensated by the quick increasing of angular speed.

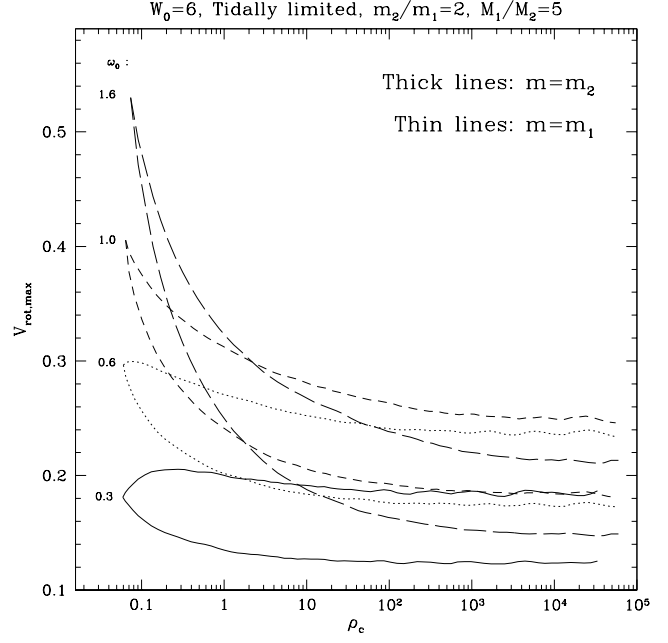


Figure 9. Evolution of the maximum rotational velocity at the equator according to the central density for models with $W_0 = 6$ and mass function of M2A. We have shown only for four different initial rotations out of 9 models. The thin lines and the thick lines represent the evolution of the lighter component and that of massive component, respectively.

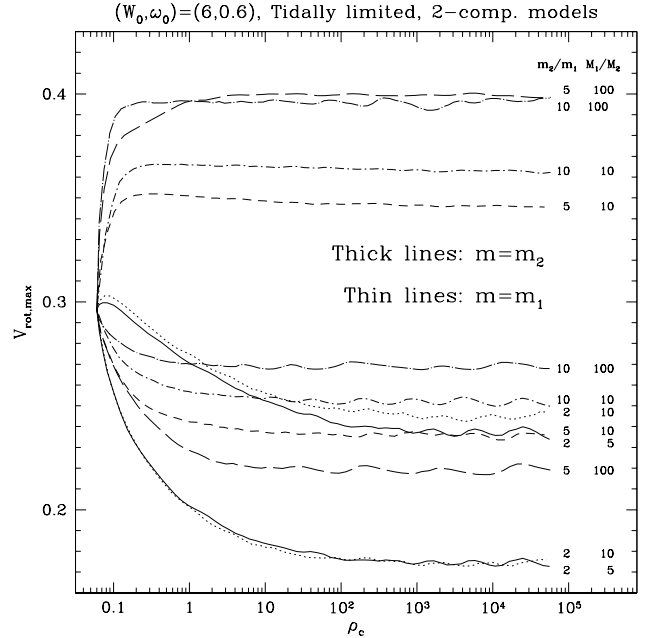


Figure 10. Same as the Fig. 9 but for all two-component models with $\omega_0 = 0.6$ of present study. The $V_{rot,max}$ of the massive stars for the models with higher individual mass ratio (m_2/m_1) even increases very fast during the early evolutionary stage due to the transfer of the angular momentum from the lighter stars.

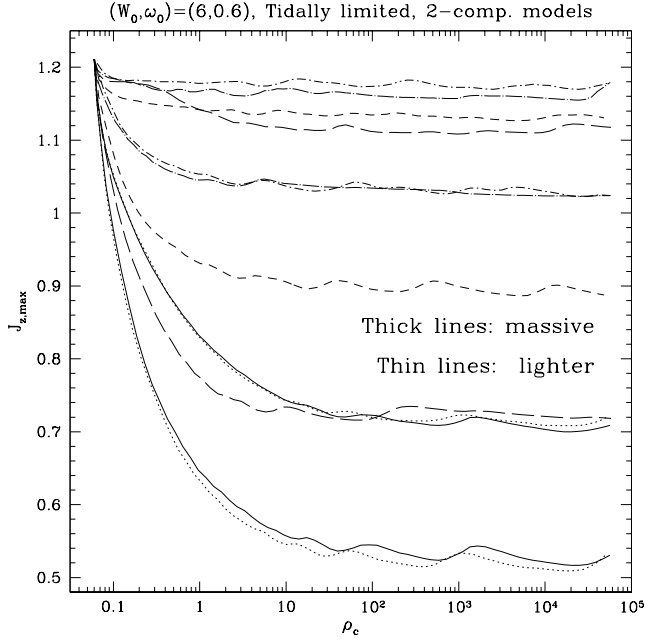


Figure 11. Evolution of the maximum specific angular momentum at the equator for the cluster model with two-component mass functions. The meaning of the line styles are the same to those of Fig. 3-10.

4 CLUSTERS WITH CONTINUOUS MASS SPECTRUMS

4.1 Evolution of central properties

Fig. 12(a) and (b) shows the time evolution of the total central density for cluster models with mass functions MCA, MCB and MCC. For each mass function three models with the different initial rotation are plotted together. Since we select the continuous mass function of the power-law type and the index of power-law varies with time due to difference in mass evaporation rates among different mass groups, we distinguish the initial power-law index (α_0) with the power-law index (α) at time t . The values of the initial power-law index are shown in figure and the models with the same mass function are connected with lines for clarity.

Like single component or two-component models, the models with the higher initial rotation evolve more rapidly than the those with lower initial rotation. Among the models with the same amount of the initial rotation the cluster with the flatter initial mass function ($\alpha_0 = -1.20$) has a longer collapse time, when the time is measured in the initial half-mass relaxation time. For models without initial rotation it is known that the core-collapse time for cluster with steeper mass function is shorter than that for the cluster with shallower mass function (e.g., Lee, Fahlman & Richer 1991; Lee & Goodman 1995; Takahashi 1997).

We have shown the evolution of the central one dimensional velocity dispersions and the central angular speeds of individual mass components for the with $(W_0, \omega_0) = (6, 0.6)$ and the initial power-law slope $\alpha_0 = -2.35$ in Fig. 13. The evolution starts at lower left corner as marked by a starry point in each figure. The individual mass of each mass group decreases upward in σ_c versus ρ_c , and vice versa for Ω_c ver-

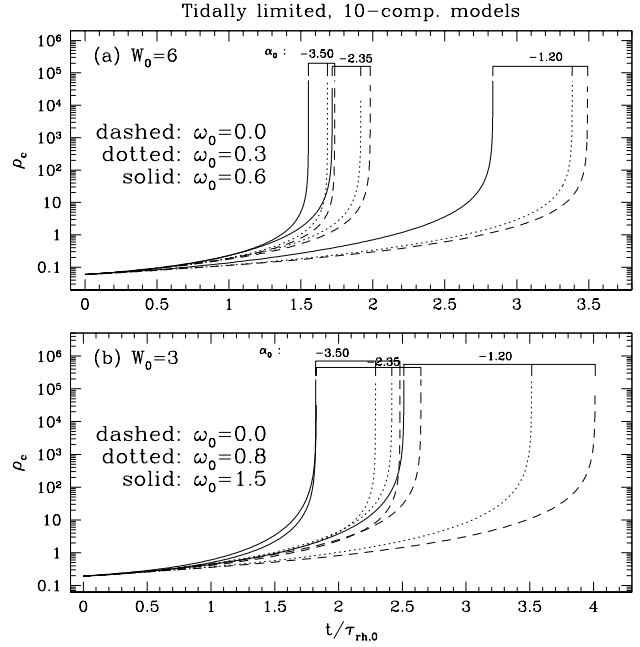


Figure 12. Time evolution of the central density for the cluster model with the central concentration $W_0 = 6$ (a) and 3 (b) and continuous mass function (10 mass components). Three different initial rotation are considered. The cluster models with the same mass function and different initial rotation is connected with a line. The acceleration of the core-collapse due to the initial rotation is shown clearly for all models.

sus ρ_c as shown in Fig. 13. The parameters γ and δ which characterize the core-collapse phase as defined in Eqs. (10) and (11) are $\gamma = 0.103$ and $\delta = 0.113$.

The effects of the initial mass function on the central velocity dispersion and the central angular speed are shown in Figs. 14 15, respectively. We keep the scales of the horizontal axis and the vertical axis to be the same for all panels. The direction for the increase of mass of each mass group is indicated by arrows in the figures. For most massive component as α_0 decreases σ_c decreases more rapidly, driving more rapid evolution of the cluster as indicated by earlier core-collapse. The development of the mass segregation is established more quickly for the model with the steeper mass function. For Ω_c versus ρ_c (Fig. 15) we have shown only the early stage of evolution since the rotation affects mainly during the initial period. It is evident that the development of self-similar core-collapse phase occurs earlier for the model with the steeper mass function than that with flatter mass function. The central angular speed at a given central density is larger for the model with the steeper mass function. The rapid increase of the central angular speed for the highest mass group and the slow decrease for the lowest mass group for the model with $\alpha_0 = -3.50$ is a consequence of the rapid development of mass segregation. The steep decrease of central velocity dispersion drives the increase of the central angular speed because of negative specific moment of inertia.

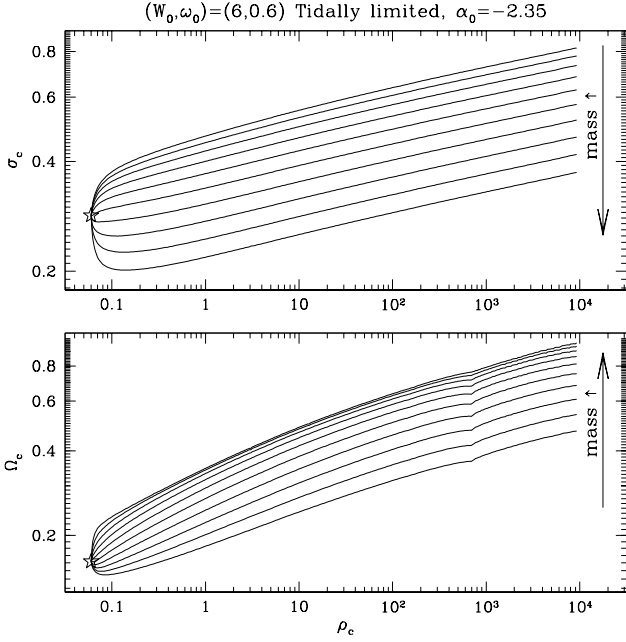


Figure 13. Evolution of the 1D central velocity dispersion (a) and the central angular speed (b) of the individual mass components for a cluster model with $(W_0, \omega_0) = (6, 0.6)$ and a power-law mass function with index $\alpha_0 = -2.35$. The staray marks denote the start of evolution. Not only the velocity dispersion, but the central angular speed shows a self-similar behaviour.

4.2 Rotational properties

Fig. 17 displays the evolution of the maximum rotational velocities of individual mass components at the equator for the model with $(W_0, \omega_0) = (6, 0.3)$. We included the models with mass functions MCA, MCB and MCC together. The total mass of each mass group increases along the arrow shown in Fig. 17(a). The evolution of rotational speed for the cluster with the continuous mass function is similar to that of the two component models. For the model with $\alpha_0 = -3.50$ the maximum rotational speed of the mass component of m_5 remains nearly a constant. Since the radius where the rotational velocity becomes maximum at the equator decreases with the time, the mass group with m_5 rotates faster with time. The constant behaviour of the maximum rotational speed occurs for the mass group of m_7 for model with $\alpha_0 = -2.35$ and mass group m_9 for model with $\alpha_0 = -1.20$, respectively. Fig. 16(a) and (b) show the evolution of the maximum rotational speed and the evolution of the maximum angular momentum at equator for model with $(W_0, \omega_0) = (6, 0.6)$ and mass function with $\alpha_0 = -2.35$. The maximum rotational speed of the lower mass groups decreases more than the cluster rotating slowly (see Fig. 17(b) for comparison). While the high mass component rotates faster, the angular momentum decreases continuously through whole evolutionary phase. Since the outward transfer of angular momentum for each mass species is closely related with the two-body relaxation process, the evolution of the maximum of the angular momentum reaches a plateau when it is measured in the central density.

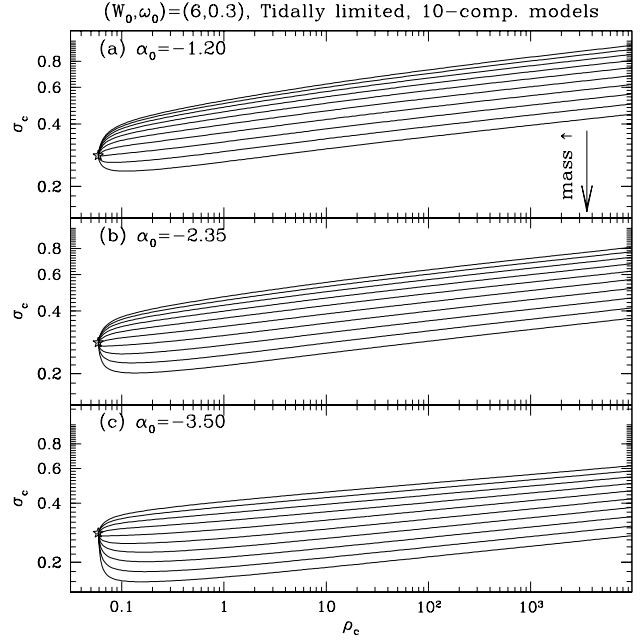


Figure 14. Evolution of the 1D central velocity dispersion for cluster models with $(W_0, \omega_0) = (6, 0.3)$ and a power-law mass function for power-law index (a) $\alpha_0 = -1.20$, (b) $\alpha_0 = -2.35$ and (c) $\alpha_0 = -3.50$, respectively. As the slope of mass function increases the central velocity dispersion of the most massive stars drops faster compared to the other mass function models. The behaviour of σ_c on ρ_c shows a self-similarity regardless of the individual mass.

5 EVOLUTION AFTER CORE-COLLAPSE

So far we have concentrated our discussion until the core-collapse. We now discuss the evolution beyond the core collapse.

5.1 Central density and mass loss

Figs. 18 and 19 show the time evolution of the central density of the rotating stellar systems beyond the core collapse. The evolutions for two component models with the central potential $W_0 = 6$ (Fig. 18(a)) and 3 (Fig. 18(b)) are displayed for clusters with three different initial rotations ($\omega_0 = 0.0, 0.3$ and 0.6 for $W_0 = 6$, and $\omega_0 = 0.0, 0.8$ and 1.5 for $W_0 = 3$). For two component clusters we employed the mass function M2C, while the mass function MCB for the continuous mass spectrum is included. The models with the largest initial rotation (solid lines) reach the collapse earlier than the models with smaller initial rotation (dashed and dotted lines). We can clearly see the acceleration of the evolution during pre and post collapse phases due to initial rotation.

Fig. 20 displays the run of the individual central density for models with the continuous mass spectrum. The mass segregation due to the energy equipartition during the early stage is shown clearly for all the present models. The run of the central density after core bounce roughly follows a power-law of $\rho_c \propto t^\beta$, for all mass groups. The index of power-law tends to be smaller for lower mass components. For the non-rotating model we find $\beta = -1.54$ for the highest mass group (m_{10}) and $\beta = -1.88$ for the

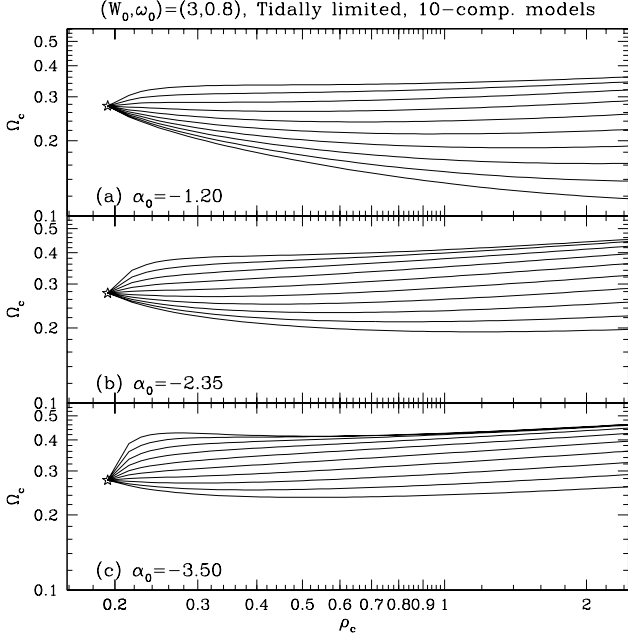


Figure 15. Evolution of the central angular speed for cluster models with $(W_0, \omega_0) = (3, 0.8)$ and a power-law mass function for power-law index (a) $\alpha_0 = -1.20$, (b) $\alpha_0 = -2.35$ and (c) $\alpha_0 = -3.50$, respectively. Evolutions during the early stage are shown since the initial rotation affects largely on the cluster dynamics during the early times.

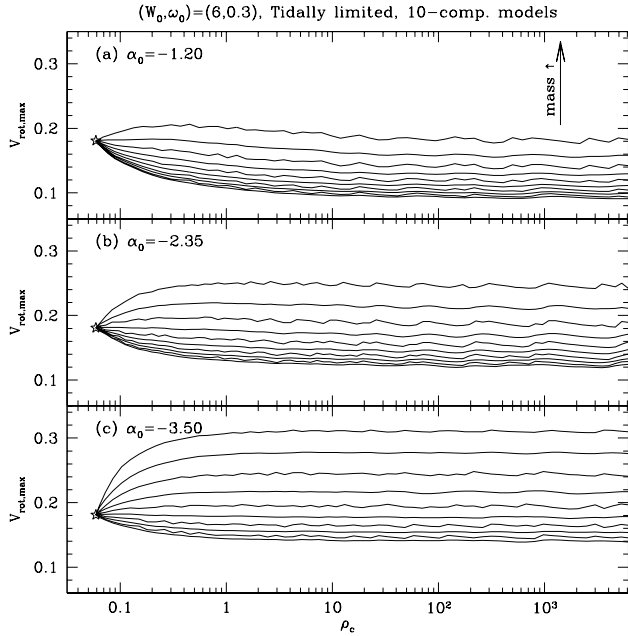


Figure 16. Evolution of the maximum rotational velocity at equator for cluster models with $(W_0, \omega_0) = (6, 0.3)$ and a power-law mass function for power-law index (a) $\alpha_0 = -1.20$, (b) $\alpha_0 = -2.35$ and (c) $\alpha_0 = -3.50$, respectively. For the steepest mass function ($\alpha_0 = -3.50$), $V_{rot,max}$ of the massive stars increase much than that of the other models with slowly increasing mass functions.

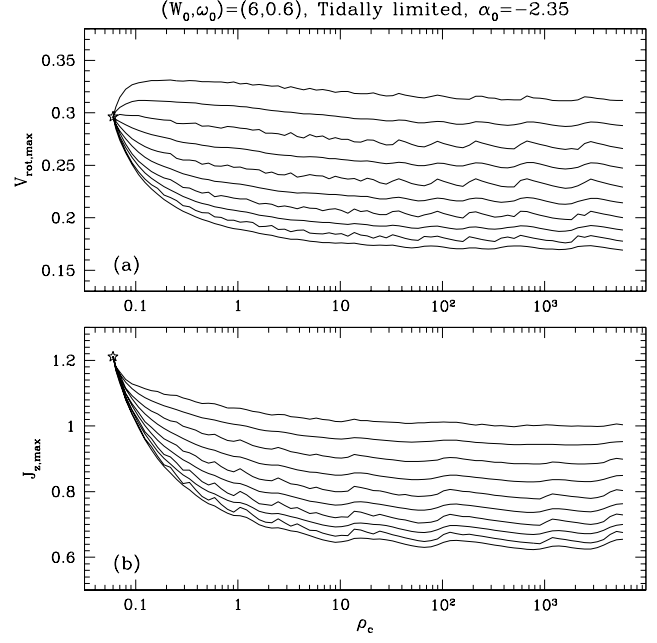


Figure 17. Evolutions of (a) the maximum rotational velocity ($V_{rot,max}$) and (b) the maximum specific angular momentum ($J_{z,max}$) at the equator for a model with $(W_0, \omega_0, \alpha_0) = (6, 0.6, -2.35)$. While $V_{rot,max}$ of the massive stars increases with time (i.e., increasing ρ_c), $J_{z,max}$ decreases monotonically due to the outward transfer of the angular momentum.

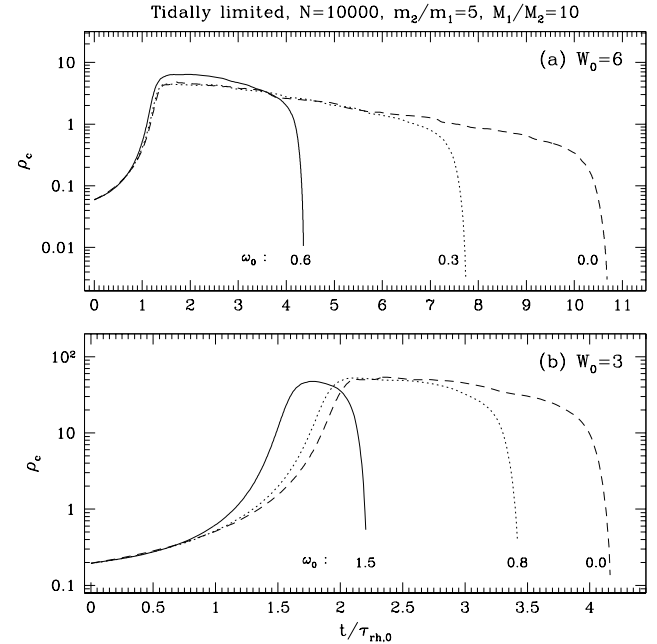


Figure 18. Evolution of the central density for the cluster models with the central potential (a) $W_0 = 6$ and (b) $W_0 = 3$ for mass function $(m_2/m_1, M_1/M_2) = (5, 10)$. The initial number of stars in a cluster is $N = 10000$ for different initial rotational parameters as indicated in the figure.

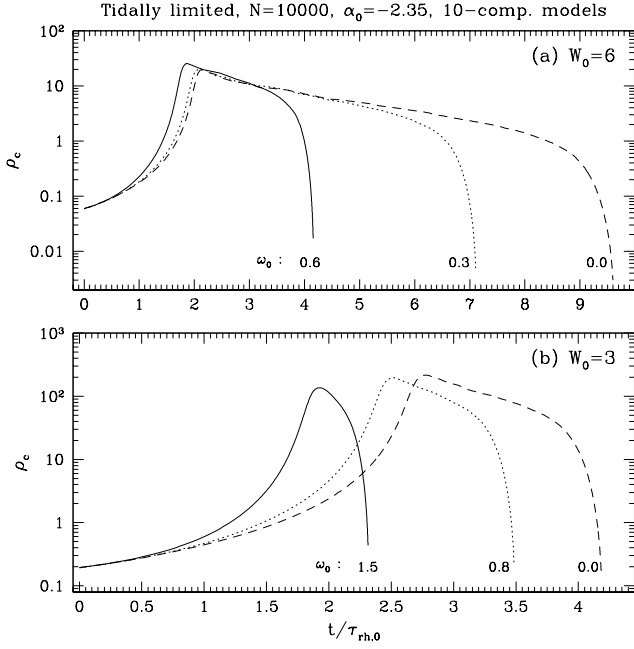


Figure 19. Same as the Fig. 18 but for models with power-law mass function ($\alpha_0 = -2.35$).

lowest mass group (m_1). These values are not far from the power law slope $\beta = -2$ of the central density with time which was derived by Kim, Lee & Goodman (1998), for two-component models. These slopes increase with the initial rotation: $\beta = -1.83$ and -2.42 for the m_{10} and the m_1 , respectively, for model with $\omega_0 = 0.6$.

We have shown the evolution of the total mass of the cluster for all post-collapse models in Fig. 21. The initial mass function, the central King’s potential and the degree of rotation are shown in each panel. The epochs of core-collapse are marked by open squares. Note the marked core-collapse time is obtained not from the present post-collapse models but from the pre-collapse models discussed in §3. Fig. 21(a) and (b) are the results obtained from two component models. The total mass of rotating cluster decrease more rapidly than the non-rotating cluster not only pre-collapse phase, but also after core-collapse. The rapid decrease of total mass for rotating model results in smaller tidal radius.

5.2 Velocity dispersion and angular speed

The evolution of the mass-weighted central velocity dispersion (σ_c) as a function of the central density (ρ_c) is shown in Fig. 22. The evolution of the central velocity dispersion after core-bounce for all post-collapse models shows a similar trend, i.e., the effect of rotation on the central velocity dispersion after core-bounce is very small. Since the core rotates like a rigid body, the rotation velocity near the cluster center is negligible. While the run of σ_c on ρ_c during pre-collapse shows the power-law behaviour due to self-similarity of collapsing core for the single mass system (Cohn 1980, Kim et al 2002), the stellar system with mass spectrum does not show a simple power-law in the early phase as explained in Sect. 3.2, due to the mass segregation. The behaviour of σ_c

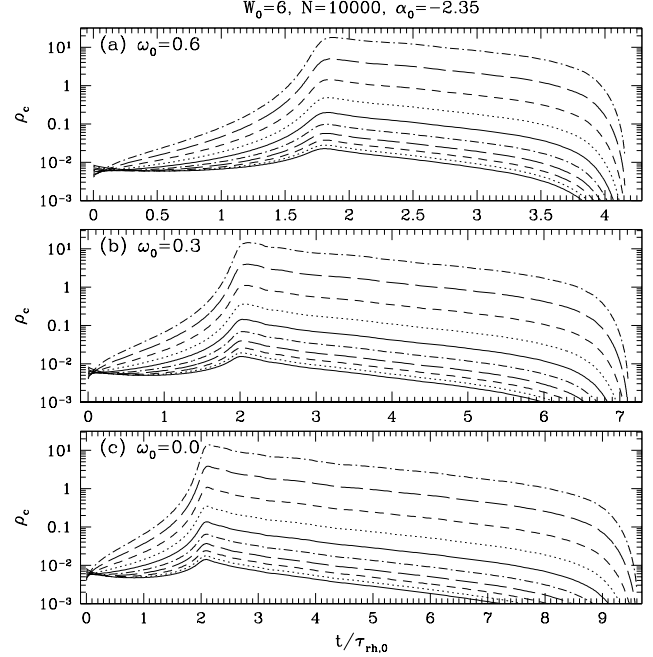


Figure 20. Time evolution of the central density of the individual mass component for models with $(W_0, \alpha_0, N) = (6, -2.35, 10000)$ and the initial rotations of (a) $\omega_0 = 0.6$, (b) $\omega_0 = 0.3$ and (c) $\omega_0 = 0.0$, respectively. ρ_c of the massive stars increases very quickly due to the development of the mass segregation.

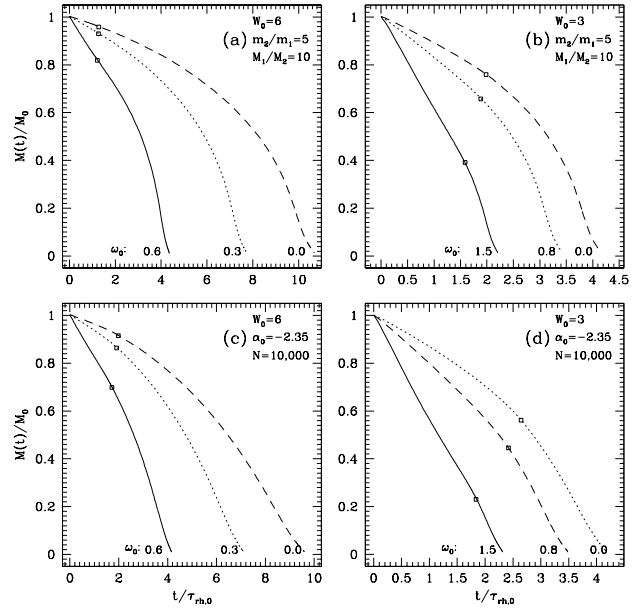


Figure 21. Evolution of the total mass retained in a cluster. The parameters characterize the cluster model are written on the upper-right corner of the each panel. The epochs of core-collapse are marked with the open squares.

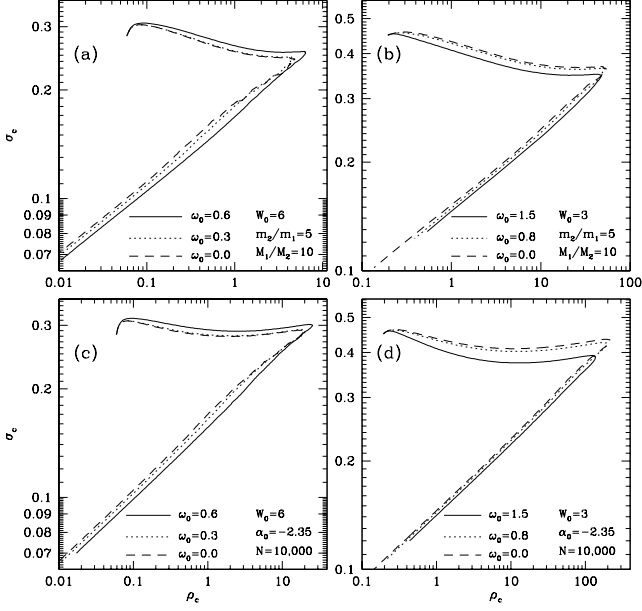


Figure 22. Evolution of the mass-weighted 1D central velocity dispersion on the central density. The model clusters shown here are the same to the models displayed in Fig. 3-21. The behaviour of σ_c on ρ_c after core-bounce shows a power-law signature irrespective of the amount of the initial rotation.

on ρ_c after core-bounce can be, however approximated as a simple power-law even for the multi-mass systems because the mass-segregation was already established at the time of the beginning of the expansion. The power-law index γ can be predicted by applying energy balance argument (Kim et al. 2002). Inspection of Fig. 22 shows $\gamma \sim 0.42$, slightly smaller than the power-law index of ~ 0.33 obtained for the single mass system.

In Fig. 23, we have shown the run of the mass-weighted central angular rotational speed (Ω_c) on the central density (ρ_c) for the whole post-collapse models which have the initial rotation. The angular speed also appears to follow roughly power law on ρ_c during both pre- and post-collapse, except for the early evolutionary stage in the pre-collapse phase for the models with $W_0 = 3$. The evolutions of Ω_c on ρ_c after the very early stage shows a similar trend irrespective of the degree of the initial rotation. It implies that the effect of the initial rotation for the cluster center disappears quickly. The evolutions of σ_c and Ω_c on ρ_c of the individual mass component for models with the continuous mass spectrum is displayed in Fig. 24. The run of σ_c is represented well by a simple power-law. The higher the stellar mass, the shallower the power-law index. While the mass-weighted central angular rotation speed appears to show the power-law behaviour on ρ_c , Ω_c of the low mass stars deviates from the power-law type evolutionary behaviour during post-collapse phase. It shows much steeper decrease than higher mass components, though the contribution of the lower mass component on the total Ω_c is negligible.

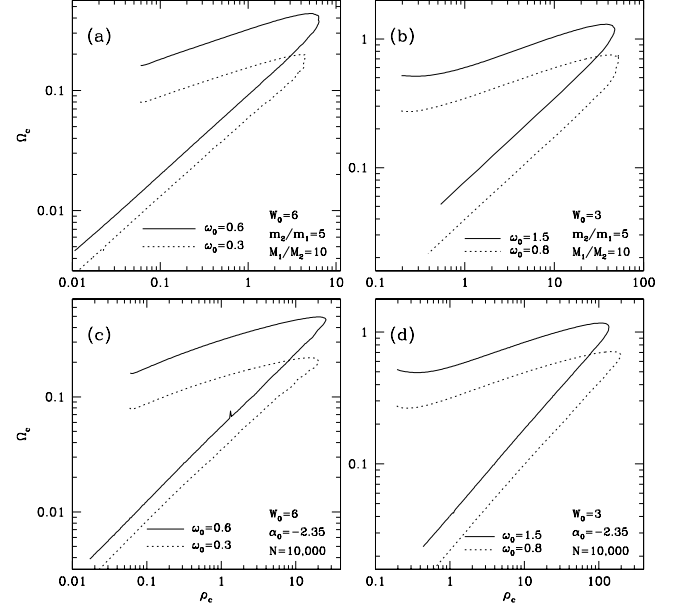


Figure 23. Same as the Fig. 22, but for mass-weighted central angular speed on the central density. Only rotating models are shown here. A small spike shown in figure (c) is mainly due to the numerical error.

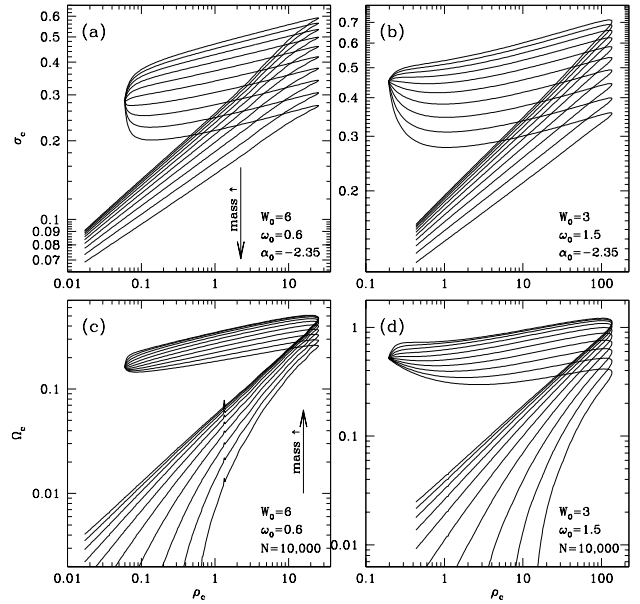


Figure 24. Evolution of the central velocity dispersion (a,b) and the central angular speed (c,d) of the individual mass component for model clusters with the fastest initial rotation ($\omega_0 = 0.6$ for $W_0 = 6$ and $\omega_0 = 1.5$ for $W_0 = 3$). In σ_c on ρ_c plots, the individual mass component show a power-law behaviour, though the index of the power-law depends on the mass of the individual star. The direction increasing individual mass is denoted with arrows in panel (a) and (c), respectively.

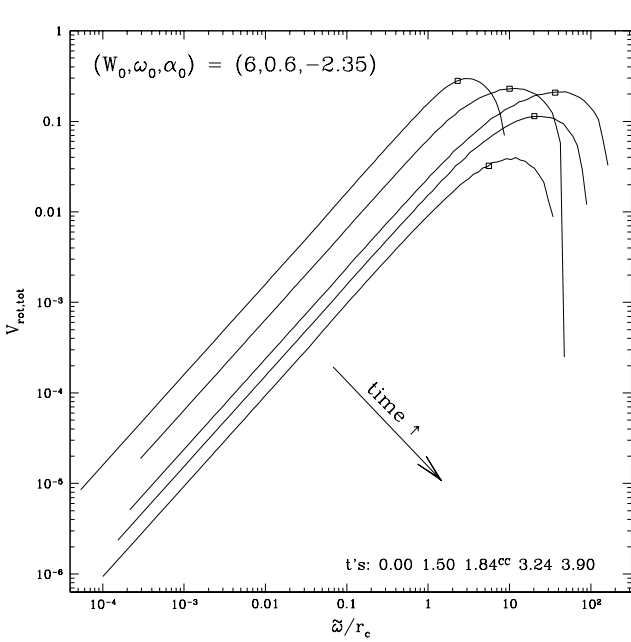


Figure 25. Radial profiles of the rotational velocities at a few selected epochs for a cluster model with $(W_0, \omega_0, \alpha_0) = (6, 0.6, -2.35)$. Half-mass radii (r_h) at corresponding epochs are marked with open squares. At the initial time, the rotational inside r_h follows a rigid body rotation. Note that the radii is measured with the current core radii.

5.3 Rotational profiles

In Figs. 25 and 26, we have shown the radial profiles of the rotational velocity at equator for model with $(W_0, \omega_0) = (6, 0.6)$ and continuous mass spectrum with $\alpha_0 = -2.35$. The run of the rotational velocity for the selected mass components (m_1, m_4, m_7, m_{10}) is displayed in Fig. 26. Epochs shown in this plot are $t/\tau_{rh,0} = 0.00, 1.50, 1.84, 3.24$ and 3.90 , where the core-collapse occurs at $t/\tau_{rh,0} = 1.84$. At $t/\tau_{rh,0} = 3.90$ the cluster is nearly completely dissolved. The half-mass radii at these each evolutionary times are marked with open squares and the direction with increasing times is shown with arrow in Fig. 25. Note that x-axis, i.e., radius of cylindrical coordinate is measured in units of the current core radius.

Total rotational velocity decreases continuously with time due to the loss of the angular momentum through the cluster boundary. The outward transfer of the angular momentum causes the increase of the radius when it is measured in units of current core radius, where the rotational velocity becomes the maximum. The radius of maximum rotational velocity decreases after core bounce due to the higher mass-loss. While the changes of angular momentum due to the outward transfer and the loss through the cluster boundary changes the structure of the velocity profile beyond the half-mass radii, the shape of rotational velocity inside the cluster core remains to be rigid body rotation.

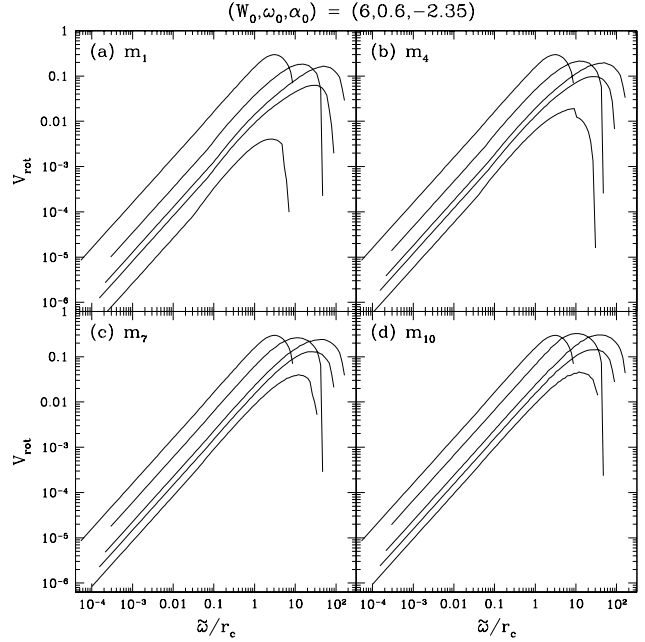


Figure 26. Same as the Fig. 25 but for a few selected mass components, (a) the lowest mass component m_1 , (b) m_4 , (c) m_7 and (d) m_{10} , the most massive star. The rotational structure of the massive stars extends farther than that of the less massive stars.

5.4 Evolution of mass function

Mass segregation drives the concentration of the higher mass stars in the cluster center while the lower mass stars go to the outer halo of the cluster. This leads to the preferential evaporation of lower mass stars through the tidal boundary. Therefore, low mass stars are selectively depleted from the initial mass function, resulting a change of the mass function with time. Near the end of the evolution, the mass function can even be inverted, i.e., there are more high mass stars than lower mass stars. The global mass function $\phi(m)$ at several selected epochs for four different models with the continuous mass spectrum is displayed in Fig. 27. We include the non-rotating models and the rapidly rotating models in order to study the effect of the initial rotation on the mass function. The shape of the mass function at the time of core-collapse is distinguished by dashed line from the mass function at the other epochs. The evolution of power-law index ($\alpha(M)$) for whole post-collapse models with the continuous mass spectrum is shown in Fig. 28. The mass function deviates from the power-law as a result of mass-dependent evaporation rates. In Fig. 28, we have shown the typical error of the fitted power-law index for the models which has the highest initial rotation. The epochs where the core-collapse occurs is marked with open squares. In the figures, we have chosen M/M_0 for the abscissa instead of time because the life-time of clusters are significantly different for different models.

It is evident that the behavior of α does not depend sensitively on the degree of rotation, although the rotation causes less change of α . Although the effect is small, the rotation causes slower changes in α as a function of M/M_0 . The

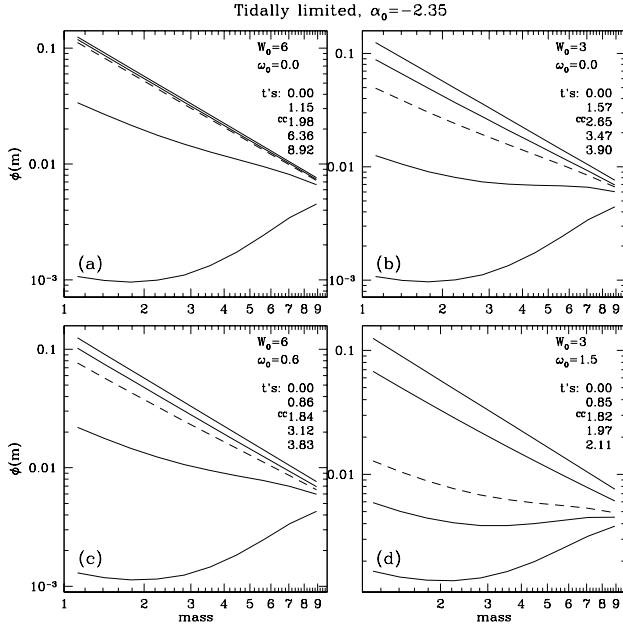


Figure 27. Mass functions of the several selected epochs for the cluster models with the continuous initial mass function with a power-law index $\alpha_0 = -2.35$. For a comparison clusters without the initial rotation (Figs. a and b) and the clusters with the highest rotation (Figs. c and d) for a given central potential are displayed. The epochs where the core-collapse happened are distinguished with dashed lines from the other evolutionary epochs. The change of mass function measured by the power-law index as a function of the cluster mass in units of initial mass is shown in next figure Fig. 28).

angular momentum exchange among different mass species appears to act against the mass segregation.

The mass function also becomes dependent on the location as the mass segregation proceeds. The existence of initial rotation and its outward transfer also affect the energy exchange process that causes mass segregation. In order to see the role of rotation on the mass segregation, we have compared the evolution of α at four different locations in Fig. 29. The different locations are chosen such that $r < r_c$, $r < r_h$, $r_h < r < 2r_h$ and $2r_h < r < 3r_h$. The slope of mass function inside the core (Fig 29a) increases with time during pre-collapse evolution. At the time of the core-collapse the shape of the mass spectrum become inverted for all models. The power-law index α at this evolutionary stage remains ~ 1.3 with a weak dependence on the the degree of the initial rotation. The mass function within the half-mass radius is flattened continuously with the decrease of total mass. The model without the initial rotation has a rather shallower mass function at fixed total mass compared to that of the cluster rotating fast. Initial rotation plays an important role in removing the stars through the tidal boundary including both the lower and higher mass stars. Compared to non-rotating models, high mass stars in rotating models appear to have higher chance of evaporation. Thus the mass function changes more slowly for rotating models than non-rotating models. Since the effect of the initial rotation remains in region $r_h < r < 2r_h$, it is expected that the shapes

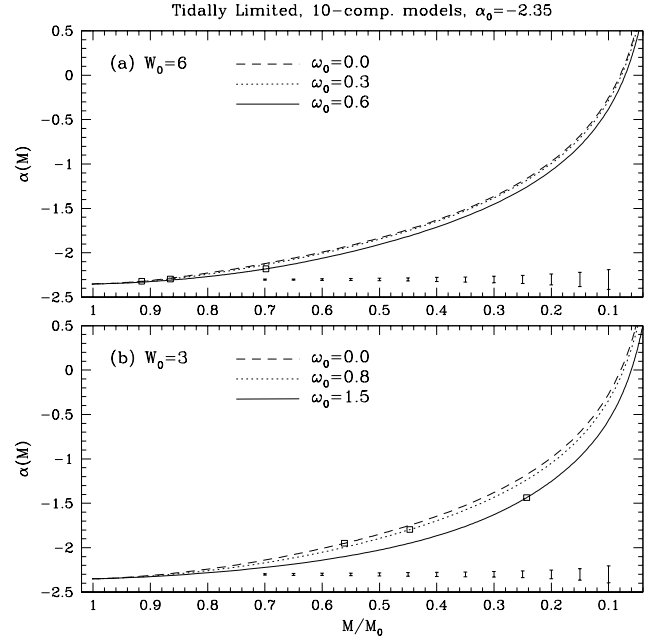


Figure 28. Evolution of the power-law index α_M on the total cluster mass for whole post-collapse models with a continuous mass function. Open squares represent the core collapse times for each cluster model. The errorbar on each panel represent the typical rotating model when performing a linear least square fitting for a double logarithm plot such as the panels in Fig. 27. The slope of the power-law mass function for a cluster with the fastest initial rotation is slightly lower than that of non-rotating model.

of mass function in this region shows significant dependence on rotation. The concentration of the high mass component in the cluster center drives the steepening of the mass function near the half-mass radius. When the development of mass segregation is settled in, the slope of the mass function decreases with time due to the selective evaporation of the lower mass stars through the tidal radius. The evolution of α for the highly rotating model shows a different profile compared to that of non-rotating model at this radial region. While there is a central concentration of the massive stars, the angular momentum which has the maximum around r_h pushes the high mass stars outward. Therefore, there is only a little change in α during the early evolutionary stage for rapidly rotating models.

6 CONCLUSION AND DISCUSSION

We have studied the dynamical evolution of the rotating stellar systems with the mass spectrum by solving the orbit-averaged 2D FP equation in (E, J_z) space. Numerical simulations are performed both for simple two component clusters and for clusters with a power-law mass function represented by ten mass species. In order to explore the evolution after core collapse we add the heating by three-body processes. We have employed rotating King models as initial models, where the velocity dispersions for all mass components are equal, i.e., no mass segregation at the begin-

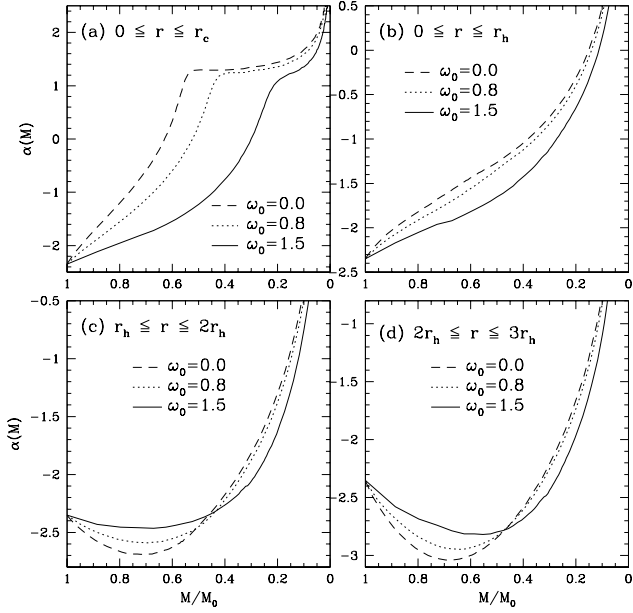


Figure 29. Same as the Fig. 28 but for four different radial regions of cluster models with the central concentration $W_0 = 3$, (a) $r < r_c$, (b) $r < r_h$, (c) $r_h < r < 2r_h$ and (d) $2r_h < r < 3r_h$, respectively. A combined effect due to the mass segregation and the initial rotation is shown clearly in panels (c) and (d).

ning. The rotating King models are characterized by two parameters: initial central potential (W_0) and degree of initial rotation (ω_0). Clusters with two different central potential $W_0 = 6$ and 3 are studied extensively. For models only until core-collapse, we have studied the evolution of the clusters with six different mass functions for two-component models, while three models are studied for clusters with a continuous mass function (power-law). For models where the evolution beyond the core-collapse are explored, we consider clusters with a mass function M2C ($m_2/m_1 = 5$, $M_1/M_2 = 10$) for the two component model and clusters with $\alpha_0 = -2.35$ for the model with continuous mass spectrum.

Our results show that, as in equal mass system, the presence of the initial rotation accelerates the dynamical evolution as manifested by rapid core collapse and dissolution. The degree of the acceleration depends on the amount of the initial rotation and the shape of mass function. As the ratio of the mass (m_2/m_1) increases the degree of the acceleration decreases for two component models since both mass segregation and the rotation compete in acceleration of core-collapse. If m_2/m_1 is very large, the mass segregation alone could significantly reduce the core-collapse time and there is not much room for rotation to accelerate further. For models with the power-law mass function, the acceleration rate of core-collapse due to the rotation is larger for the model with a steeper slope of the mass function for a given initial rotation parameter (ω_0). The shortening of the life-time (dissolution of cluster) due to the rotation is observed far beyond the core bounce. The increase of mass loss rate, resulting from the enhanced two-body relaxation process causes the faster dissolution of cluster.

The evolution of σ_c on ρ_c can be approximated by a

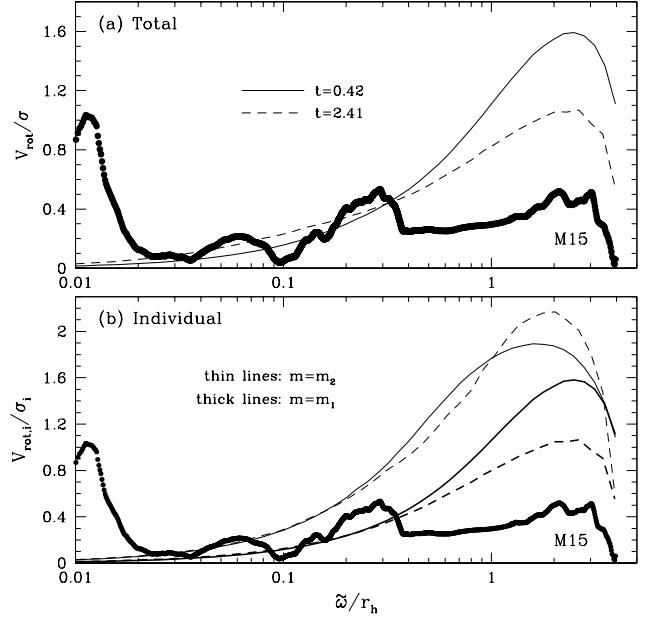


Figure 30. Comparison of observed radial profile of the rotational velocity over 1D velocity dispersion for the galactic globular cluster M15 (data provided by Gebhardt 2002) with the result of a selected two-component model with $(W_0, \omega_0) = (6, 0.6)$, $(m_2/m_1, M_1/M_2) = (5, 10)$.

power-law except for the early evolutionary stage regardless of the degree of rotation both for pre- and post-collapse. The measured power law index γ for pre-collapse is very close to the value obtained for single mass system, while we have obtained a slightly shallower slope for post-collapse phase. The development of mass segregation, a consequence of the evolution of the multi-mass system is visible clearly both for non-rotating and rotating models. The evolution of Ω_c on ρ_c shows a power-law behaviour, too. The slope of the power-law is, however, larger than that obtained for the single mass cluster. While the angular momentum is transferred only outward for the equal mass system, the exchange of the angular momentum between different mass species occurs for the multi-mass system, resulting a faster increase of Ω_c on ρ_c . Due to a cooperation of the central concentration of the massive stars (mass segregation) and the transfer of angular momentum from high mass to low mass stars, the radii where V_{rot} reaches the maximum value goes outward. The maximum rotation of the most massive stars even increases at the early times, while it shows a monotonic decrease for the single mass system.

There are a few observations regarding the direct measurement of the rotation parameter (V_{rot}) (Gebhardt et al. 1995). Recently Gerssen et al. (2002) reported the kinematical study of the central part of the globular cluster M15, including V_{rot} . M15 is known as the globular cluster which contains a collapsed core. The radial profile of V_{rot}/σ (rotational velocity over one dimensional velocity dispersion) shows a steep increase and a rapid decline followed by a slow rise. The steep rise of V_{rot}/σ near the cluster center can not be explained by a single mass model (Kim et al. 2002). We have shown the run of V_{rot}/σ for two compo-

nent model in Fig. 30 at two selected epochs, one in pre-collapse ($t/\tau_{rh,0} = 0.42$) and the other after core bounce ($t/\tau_{rh,0} = 2.41$), together with the observed data by Gebhardt (2002). The radius is measured in current half-mass radius. It is evident that cluster loose the angular momentum through the tidal boundary. The behaviour of the mass-weighted V_{rot}/σ (Fig. 30(a)) are roughly similar to that of observed profile of M15 except for the central region. Note that the known half-mass radius of M15 is ~ 3.09 (Djorgovski 1993). For the high mass component, $V_{rot,i}/\sigma_i$ where i represents the individual mass component, at $t = 2.41$ is higher than that obtained at $t = 0.42$, especially beyond r_h . It is mainly due to the lower velocity dispersion after core bounce, not due to the higher value of the rotation velocities. The highly rotating central region of M15 is, as in single mass system, not explained with the current multi-mass models, although there is difference in rotational structure between the single mass and the multi-mass systems. From the kinematical study of the central region of M15, Gerssen et al. (2002) proposed the presence of intermediate mass black hole (IMBH) with $M = 3.9 \times 10^3 M_\odot$. On the contrary, Baumgardt et al. (2002) demonstrated that the rise of velocity dispersion into the center can be explained with the clustering of the remnant stars, which are expected to be overwhelmingly populated in the cluster core than the normal stars. However, they did not rule out the possibility of the presence of IMBH. It may be necessary to include the remnant stars and the IMBH in current 2DFP models to investigate the role of the initial rotation on the observed strong increasing of V_{rot}/σ near the center of M15.

The models presented here still neglect many important physical processes occurring in real star clusters. The stellar evolution and primordial binaries are known to affect the early evolution of globular clusters. The possible existence of intermediate mass black hole in the center could also affect the course of dynamical evolution. These will be the task of future works.

This work was supported by the Korea Research Foundation Grant No. D00268 in 2001 to HML and by SFB439 to RS.

REFERENCES

- Anderson, J. & King, I.R., 2003, ApJ, 126, 772
 Baumgardt, H., Hut, P., Makino, J., McMillan, S.L.W., & Portegies Zwart, S., 2002, ApJ, 582, L21
 Cohn H., 1979, ApJ, 234, 1036
 Cohn H., 1980, ApJ, 242, 765
 Djorgovski, S. G., 1993, in Structure and Dynamics of Globular Clusters, eds. S. G. Djorgovski and G. Meylan, Astronomical Society of Pacific, p373
 Einsel C., Spurzem R., 1999, MNRAS, 302, 81
 Fregeau, J.M., Joshi, K.J., Portegies Zwart, S.F., & Rasio, F.A., ApJ, 2002, 570, 171
 Gao, B., Goodman, J., Cohn, H., & Murphy, B., 1991, ApJ, 370, 567
 Gebhardt, K., 2002, private communication
 Gebhardt, K., Pryor, C., Williams, T. B., & Hesser, J. E., 1995, AJ, 110, 1699
 Gerssen, J., van der Marel, R. P., Gebhardt, K., Guhathakurta, P., Peterson, R., & Pryor, C., 2003, ApJ, in press.
 Giersz, M., & Spurzem, R., 2000, MNRAS, 270, 700
 Goodman J., 1983, Ph.D. Thesis, Princeton University
 Goodman J., 1987, ApJ, 313, 576
 Khalisi, E., Doctoral Thesis, Univ. Heidelberg, 2002, <http://www.ub.uni-heidelberg.de/archiv/3096>
 Kim, E., Einsel, C., Lee, H. M., Spurzem, R. & Lee M. G., 2002, MNRAS, 334, 310
 Kim, S. S., Lee, H. M. & Goodman, J., 1998, ApJ, 495, 786
 Lee, H. M., Fahlman, G. & Richer, H., 1991, ApJ, 366, 455
 Lee, H. M. & Goodman, J., 1995, ApJ, 443, 109
 van Leeuwen, F., Le Poole, R.S., Reijns, R.A., Freeman, K.C., & de Zeeuw, P.T., 2000, A&A, 360, 471
 Lupton, R.H., & Gunn, J.E., 1987, AJ, 93, 1106
 Portegies Zwart, S.F., Takahashi, K., 1999, CeMDA, 73, 179 Princeton Univ. Press
 Spitzer L. Jr. & Hart M. H., 1971, ApJ, 164, 399
 Spurzem R., Einsel C., 1998, in D.R. Merritt, M. Valuri, J.A. Sellwood, eds, Massive Stellar Clusters, ASP Conf. Ser. No. 182, ASP: San Francisco, p. 105.
 Takahashi, K., 1995, PASJ, 47, 561
 Takahashi, K., 1996, PASJ, 48, 691
 Takahashi, K., 1997, PASJ, 49, 547
 Takahashi, K. & Lee, H. M., 2000, MNRAS, 316, 671
 Takahashi, K., Lee, H. M. & Inagaki, S., 1997, MNRAS, 292, 331
 Takahashi, K., & Portegies Zwart S.F., 1998, ApJL, 503, L49
 White E.R., Shawl J.S., 1987, ApJ, 317, 246